SIMULATION OF WATER FLOW IN DOUBLE-POROSITY SOILS ON UNSTRUCTURED GRIDS WITH THE FINITE-VOLUME METHOD

ADAM SZYMKIEWICZ[1] AND KAZIMIERZ BURZYŃSKI[2]

[1] Institute of Hydroengineering, Polish Academy of Sciences,
Kościerska 7, 80-328 Gdansk, Poland
adams@ibwpan.gda.pl

[2] Gdansk University of Technology,
Faculty of Civil and Environmental Engineering,
Narutowicza 11/12, 80-952 Gdansk, Poland

Abstract: Double-porosity soils consist of two interacting porous systems corresponding to weakly conductive aggregates and highly conductive inter-aggregate regions. The flow of water in such media can be described with a two-scale model obtained by homogenization. The model consists of a single macroscopic equation for the flow in the highly conductive porous system coupled with a number of micro-scale equations for the flow in the weakly conductive aggregates. In this paper we present a numerical algorithm to solve the resulting system of equations for the case of macroscopically two-dimensional flow. It is based on the finite volume approach for unstructured grid of triangular cells. Special attention is paid to the coupling of the micro- and macro-scale equations. An exemplary calculation is presented, concerning infiltration and redistribution of water in a hill-slope of double-porosity structure with cubic aggregates.

Keywords: double-porosity soils, Richards equation, unsaturated zone, finite volume method, unstructured grid

1. Introduction

Numerical simulations of soil water flow are required in many civil engineering applications, including prediction of such risks as groundwater contamination or slope failure. The flow of water in a partially saturated porous medium is routinely described with the following Richards equation:

$$\frac{\partial \theta(h)}{\partial t} - \nabla_x \cdot (\boldsymbol{K}(h)\nabla(h+z)) = 0. \tag{1}$$

In Equation (1), h is the water potential head, which assumes negative values under unsaturated conditions, θ is the volumetric water content, $\boldsymbol{K}$ is the hydraulic conductivity tensor, t is time and $\boldsymbol{x} = (x,y,z)^T$ is the spatial variable, z being oriented positively upwards. Equation (1) is nonlinear and the solution requires the knowledge

of its constitutive functions, *i.e.* the relations between the potential head, water content and conductivity. Their form depends on the type of the porous material.

In this paper we consider double-porosity soils, an example of heterogeneous porous media. Such soils, often encountered in nature, contain aggregates of fine-grain material with very small pores, while the space between the aggregates is filled with coarse material with larger pores (see Figure 1). The constitutive functions of the two materials are very different in form and their conductivities differ by several orders of magnitude. Since the characteristic size of the aggregates is much smaller than the domain of interest, it is usually impossible to represent the heterogeneous structure explicitly in a numerical solution. An alternative approach would be to perform a kind of averaging of the constitutive functions and use the averaged functions in Equation (1), but due to large local differences in conductivity such method often produces inaccurate results. A two-scale modeling approach has been proposed in order to overcome this problem, *e.g.* [1–3], which postulates simultaneous solution of a macroscopic equation for the flow in the highly conductive system and a number of microscopic scale equations for the flow in aggregates. However, numerical implementation of such models is challenging and has received only limited attention in the literature [4, 5].

The main objective of this paper is to present a numerical algorithm for a two-scale model of unsaturated water flow in double-porosity soil. The algorithm is suitable for two-dimensional domains. It is based on the cell-centered finite-volume approach for unstructured grids proposed in [6] for the standard Richards equation. In the following sections we present the governing equations, the numerical solution algorithm and two examples of calculations.

2. Governing equations

The details of the model presented here can be found in papers [2, 3]. The medium is conceptualized as a continuous macroporous region, Ω_M, with embedded, disconnected, periodically arranged, microporous aggregates, Ω_m (see Figure 1). The volumetric fractions of the two sub-domains are respectively denoted by f_M and f_m. Two observation scales can be distinguished in such media: the macroscopic scale corresponding to the modeled domain and the microscopic scale corresponding to a single aggregate. Since the aggregates are separated from each other, at the macroscopic scale the flow occurs only in the macroporous region, Ω_M. The aggregates act as a source or sink term, absorbing or releasing water to the macroporous sub-domain, depending on the actual condition of the flow. Thus, the macroscopic flow equation has the following form:

$$f_M \frac{\partial \theta_M(h_M)}{\partial t} - \nabla_x \cdot \left[\boldsymbol{K}^{\mathrm{eff}}(h_M) \nabla_x (h_M + z) \right] + Q = 0, \qquad (2)$$

where θ_M and h_M are the water content and the water potential head in the macroporous sub-domain, $\boldsymbol{K}^{\mathrm{eff}}$ is the effective conductivity tensor and Q is the source term representing water transfer between the macroporus and the microporous regions. The effective conductivity, $\boldsymbol{K}^{\mathrm{eff}}$, depends on the conductivities of the two porous materials and on the micro-scale geometry. In a general case, it is computed from the solution of the so-called local boundary value problem, specified for the
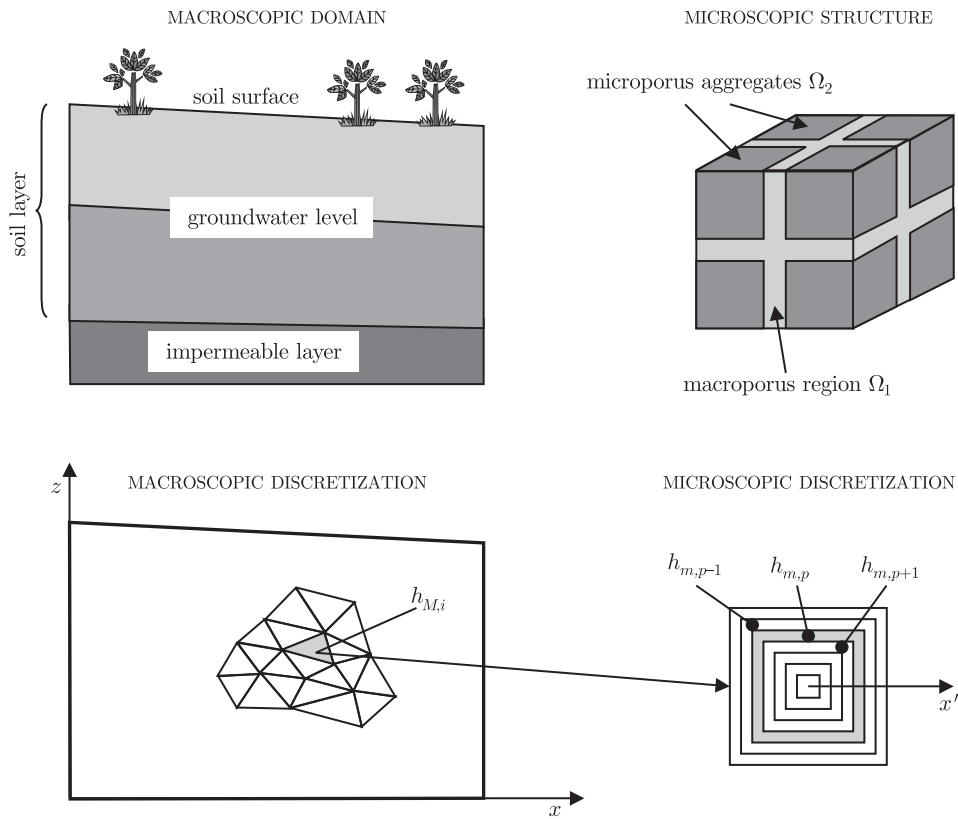
MACROSCOPIC DOMAIN

MICROSCOPIC STRUCTURE

Figure 1. General scheme of the two-scale numerical approach

given geometry of the periodic cell [3, 7]. In this paper, we consider only media that are macroscopically isotropic, *i.e.* containing cubic or spherical, isotropically-spaced aggregates. The effective conductivity for such geometry is a scalar and can be computed from the Hashin-Shtrikman formula [8]:

$$K^{\text{eff}}(h_M) = K_M(h_M) + \frac{2f_m K_M(h_M)(K_m(h_M) - K_M(h_M))}{2K_M(h_M) + f_m(K_m(h_M) - K_M(h_M))}, \tag{3}$$

where K_m is the conductivity of the microporous aggregates.

The source term Q represents the amount of water exchanged between the macropores and the aggregates. It equals the rate of change of the aggregates' average water content:

$$Q = \frac{1}{|\Omega|} \int_{\Omega} \frac{\partial \theta_m}{\partial t} d\Omega = f_m \frac{\partial \bar{\theta}_m}{\partial t}, \tag{4}$$

where $|\Omega|$ is the volume of the periodic cell and $\bar{\theta}_m$ is the average water content in the aggregates. In order to calculate the average value of water content in the aggregates, one has to consider the micro-scale flow inside a single aggregate, described by the following equation:

$$\frac{\partial \theta_m(h_m)}{\partial t} - \nabla_{x'} \cdot (K_m(h_m) \nabla_{x'} h_m) = 0, \tag{5}$$

where the $\nabla_{x'}$ operator denotes differentiation with respect to the microscopic spatial variable, $\boldsymbol{x'} = (x', y', z')$, associated with the aggregate (see Figure 1). Gravity is absent

from Equation (5). In order to compute the value of the source term at a given point $\boldsymbol{x}$ of the macroscopic domain, one has to solve Equation (5) for the aggregate associated with point $\boldsymbol{x}$. Since the water potential is continuous at the interface between the macroporous and microporous regions, the boundary condition for equation (5) is:

$$h_m(\boldsymbol{x},\boldsymbol{x'},t) = h_M(\boldsymbol{x},t) \text{ on } \Gamma, \tag{6}$$

where Γ denotes the aggregate's external surface. Equation (5) has to be solved for each cell of the macroscopic numerical grid.

3. Numerical algorithm

The model's numerical implementation requires solution of Equation (2) on a macroscopic grid and simultaneous solution of a number of micro-scale equations (5), each with its own microscopic grid. Equation (2), similarly to Equation (1), is a nonlinear partial differential equation of parabolic type and can be solved using any numerical method developed for Richards equation. In this paper, we have used the cell-centered finite volume scheme for unstructured triangular grids developed in [6]. In order to facilitate the numerical solution, the three-dimensional micro-scale equations (5) have been reduced to their one-dimensional forms as proposed in [9]. The solutions of macro and micro-scale equations have been coupled using an iterative procedure proposed in [5].

3.1. Finite-volume formulation

The macroscopic equation is solved in a two-dimensional domain, $x - z$. The domain is covered with an unstructured triangular grid (see Figure 2). Following the standard finite-volume approach, we can transform Equation (1) for each of the triangular cells into the following balance equation:

$$F_i f_M \frac{\partial \theta_M}{\partial t} + F_i f_m \frac{\partial \bar{\theta}_m}{\partial t} + L_{ij} q_{ij} + L_{ik} q_{ik} + L_{il} q_{il} = 0, \tag{7}$$

where F_i is the area of cell i, q marks the components of fluxes normal to the edges (see Figure 2) and L – the length of the respective edges. The repeating indices in Equation (7) do not represent summation. The fluxes are given by Darcy's law:

$$q_{ij} = -K^{\text{eff, av}} \frac{\partial h_M}{\partial n} - K^{\text{eff, av}} \boldsymbol{n}_z, \tag{8}$$
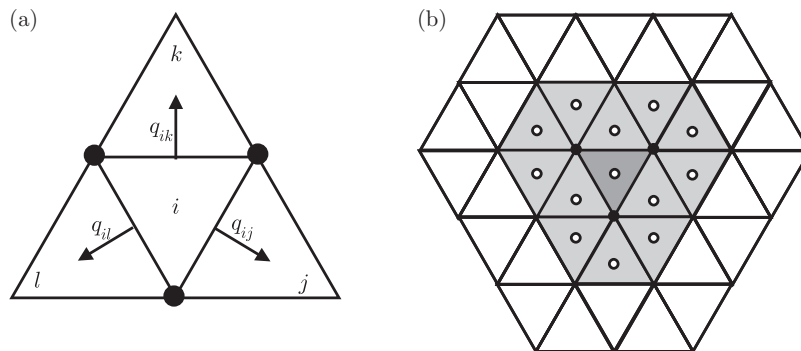

Figure 2. Discretization of the macroscopic flow equation for a single triangular cell:
(a) edge fluxes, (b) cells involved in the numerical stencil

where $K^{\mathrm{eff,av}}$ is the value of effective conductivity at the edge and $\boldsymbol{n}$ denotes the unit vector normal to the edge and oriented outwards from cell i. The potential derivative in the normal direction is approximated by a differential formula involving the cell-centered values of potential from cell i and the surrounding cells (see Figure 2). The first step of the flux approximation is a reconstruction of the potential values at the vertices.

3.2. Approximation of potential at grid vertices

The values of water potential at the vertices are expressed as linear combinations of the cell-centered values from cells sharing the considered vertex (see Figure 3). The linear coefficients are obtained with the least-squares reconstruction technique [10, 11]. Using the Taylor expansion of function h_P in the neighborhood of vertex P, we can approximate the potential values at the neighboring cell centers as:

$$h_k \approx h_{M,P} + \left.\frac{\partial h_M}{\partial x}\right|_P \Delta x_k + \left.\frac{\partial h_M}{\partial z}\right|_P \Delta z_k, \tag{9}$$

for $k = 1 \dots N_P$, where N_P denotes the set of cells sharing vertex P. In the following part, we omit the M subscript at the potential head to simplify presentation. Application of the expansion (9) to all neighboring cell centers leads to the following system of equations:

$$\begin{bmatrix} 1 & \Delta x_1 & \Delta z_1 \\ 1 & \Delta x_2 & \Delta z_2 \\ & \vdots & \\ 1 & \Delta x_{N_P} & \Delta z_{N_P} \end{bmatrix} \left\{ \begin{array}{c} h_P \\ \frac{\partial h}{\partial x}|_P \\ \frac{\partial h}{\partial z}|_P \end{array} \right\} = \left\{ \begin{array}{c} h_1 \\ h_2 \\ \vdots \\ h_{N_P} \end{array} \right\}, \tag{10}$$

or, in a more concise form:

$$\boldsymbol{AX} = \boldsymbol{B}, \tag{11}$$

where $\Delta x_k = (x_P - x_k)$, $\Delta z_k = (z_P - z_k)$. The system is over-determined. We seek the value of h_P and its derivatives that minimize $\|\boldsymbol{AX} - \boldsymbol{B}\|^2$ in the least-square sense. They can be found from the solution of the following set of normal equations [10, 11]:

$$(\boldsymbol{A}^T \boldsymbol{WA})\boldsymbol{X} = (\boldsymbol{A}^T \boldsymbol{WB}), \tag{12}$$

where matrix $\boldsymbol{W} = \mathrm{diag}(w_k)$. The components w_k of the diagonal matrix $\boldsymbol{W}$ represent the weights assigned to each of the neighboring cells. In our case, they are equal to the
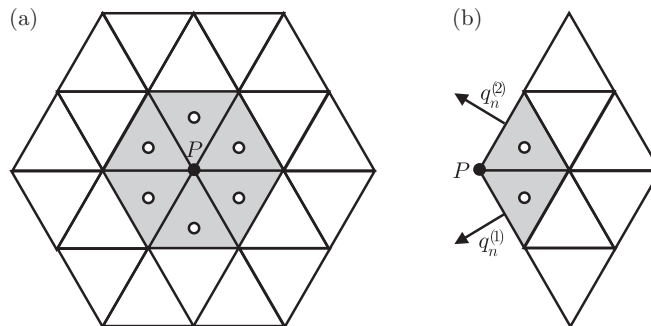

Figure 3. Numerical stencil for reconstruction of the potential head
at (a) internal and (b) boundary vertices

inverse of distance between the vertex and the center of a given cell, normalized with respect to the sum of inverses of distances from the centers of all cells surrounding P. Inverting the coefficient matrix at the left-hand side of Equation (12), we obtain the following formula for h_P:

$$h_P = \sum_{k=1...N_P} \alpha_k^{(P)} h_k, \tag{13}$$

where the $\alpha_k^{(P)}$ coefficients are constants depending on the grid's geometry. If the vertex is located at the boundary with a Dirichlet boundary condition, we simply have:

$$h_P = h^{\text{bound}}, \tag{14}$$

where h^{bound} is the value of potential imposed at the boundary. In the case of a Neumann boundary condition (see Figure 3b), system (10) should be completed with equations resulting from the imposed conditions, in the following form:

$$-K_P^{\text{eff}} \frac{\partial h}{\partial x} n_x^{(1)} - K_P^{\text{eff}} \frac{\partial h}{\partial z} n_z^{(1} - K_P^{\text{eff}} n_z = q_n^{(1)}, \tag{15a}$$

$$-K_P^{\text{eff}} \frac{\partial h}{\partial x} n_x^{(2)} - K_P^{\text{eff}} \frac{\partial h}{\partial z} n_z^{(2)} - K_P^{\text{eff}} n_z = q_n^{(2)}, \tag{15b}$$

where superscripts (1) and (2) refer to the two boundary edges sharing vertex P. The resulting formula is:

$$h_P = \sum_{i=1...N_P} \alpha_k^{(P)} h_k + \beta^{(P)}, \tag{16}$$

where $\beta^{(P)}$ depends on the boundary flux values. Conductivity K_P^{eff} depends on h_P, and thus $\beta^{(P)}$ is obtained by an iterative method.

3.3. Approximation of edge fluxes

The edge flux from cell i to cell j is defined using the diamond scheme [6] (see Figure 4a). The values of potential gradients on each side of the edge can be approximated as:

$$G_i = \frac{h_{Ei} - h_i}{d_i}, \qquad G_j = \frac{h_j - h_{Ej}}{d_j}. \tag{17}$$

The h_{Ei} and h_{Ej} values are obtained by linear interpolation of the potential values at vertices $P1$ and $P2$:

$$h_{Ei} = \frac{l_{i2}}{l_{i1} + l_{i2}} h_{P1} + \frac{l_{i1}}{l_{i1} + l_{i2}} h_{P2}, \qquad h_{Ej} = \frac{l_{j2}}{l_{j1} + l_{j2}} h_{P1} + \frac{l_{j1}}{l_{j1} + l_{j2}} h_{P2}. \tag{18}$$

The average gradient is calculated as follows:

$$G_{ij} = \frac{d_i}{d_i + d_j} G_i + \frac{d_j}{d_i + d_j} G_j. \tag{19}$$

In contrast to the approach presented in [6], the average conductivity is computed here as the arithmetic (and not harmonic) mean of the cell-centered values, which ensures better results for infiltration in dry soil [12]:

$$K^{\text{eff,av}} = \frac{1}{2} \left(K^{\text{eff}}(h_i) + K^{\text{eff}}(h_j) \right). \tag{20}$$
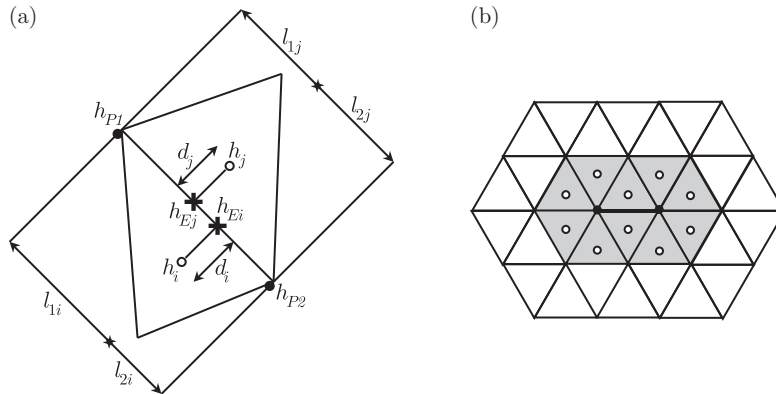
Figure 4. Approximation of edge fluxes: (a) the four-point diamond scheme,
(b) the cells involved in the numerical stencil

The vertex values of potential are given by linear combinations of the cell-centered
values of the surrounding cells, according to Equation (16). Thus, the integral of flux
along the edge, required in Equation (7), can be written as follows:

$$q_{ij} L_{ij} = -K^{\text{eff,av}} \left(G_{ij} + n_z^{(ij)} \right) L_{ij} = \sum_{k=1...N_E} \alpha_k^{(E)} h_k + \beta^{(E)}, \qquad (21)$$

where N_E is the number of cells sharing at least one vertex with the ij edge (see
Figure 4b). The $\alpha_k^{(E)}$ and $\beta^{(E)}$ coefficients depend on h_i and h_j via Equation (20).

3.4. Discretization in time and linearization scheme

Discretization with respect to time is performed using the implicit Euler scheme.
A fully discrete form of Equation (7) is obtained for each grid cell i by replacing
the time-derivative with the first-order difference approximation and introducing the
discrete approximations of the three edge fluxes given by Equation (21). The result
is the following equation:

$$f_M \frac{\theta_{M,i}^{q+1} - \theta_{M,i}^q}{\Delta t} + f_m \frac{\theta_{m,i}^{q+1} - \theta_{m,i}^q}{\Delta t} + \sum_{k=1...N_C} \alpha_k^{q+1} h_k^{q+1} + \beta_i^{q+1} = 0, \qquad (22)$$

where Δt is the time step, q is the time level index, N_C is the number of grid cells in the
stencil shown in Figure 2b, while α and β are coefficients resulting from summation
of the three fluxes given by Equation (21). Equation (22) is nonlinear as θ_M, α and
β are functions of h. Moreover, θ_m also indirectly depends on h, via the solution of
Equation (5) with boundary condition (6).

In order to solve the system of nonlinear equations arising from the dis-
cretization, we have adapted the approach proposed in [13] to the case of double-
porosity. Equation (20) has been reformulated so that the primary unknown is
the correction of the macroscopic capillary pressure head in the current iteration,
$\delta h_i^{q+1,r+1} = h_i^{q+1,r+1} - h_i^{q+1,r}$, where r is the iteration index. The following lineariza-
tion schemes have been used:

$$\theta_{M,i}^{q+1,r+1} \approx \theta_{M,i}^{q+1,r} + \left. \frac{\partial \theta_M}{\partial h} \right|_i^{q+1,r} \delta h_i^{q+1,r+1}, \qquad (23a)$$

$$\bar{\theta}_{m,i}^{q+1,r+1} \approx \bar{\theta}_{m,i}^{q+1,r} + \left.\frac{\partial \bar{\theta}_m}{\partial h}\right|_i^{q+1,r} \delta h_i^{q+1,r+1}, \tag{23b}$$

$$\sum_{k \in T_C} \alpha_k^{q+1,r+1} h_k^{q+1,r+1} + \beta_i^{q+1,r+1} \approx \sum_{k \in T_C} \alpha_k^{q+1,r} h_k^{q+1,r} + \sum_{k \in T_C} \alpha_k^{q+1,r} \delta h_k^{q+1,r+1} + \beta_i^{q+1,r}. \tag{23c}$$

The $\partial\theta_M/\partial h$ derivative in Equation (23a) can be calculated from the analytical formula describing the $\theta_M(h_M)$ relation, while the $\partial\bar{\theta}_m/\partial h$ derivative in Equation (23b) has to be computed numerically. To this end, one has to solve the micro-scale equation at the macroscopic cell i twice: first with the $h_m = h_{M,i}$ boundary condition and then with the $h_m = h_{M,i} + \sigma$ condition, where σ is a small number. Introducing Equation (23) into Equation (22) yields the following equation for $\delta h_i^{q+1,r+1}$:

$$\left(F_i f_M \left.\frac{\partial \theta_M}{\partial h}\right|_i^{q+1,r} + F_i f_m \left.\frac{\partial \bar{\theta}_m}{\partial h}\right|_i^{q+1,r} \right) \delta h_i^{q+1,r+1} + \sum_{k \in T_C} \alpha_k^{q+1,r} \delta h_k^{q+1,r+1} = R_i^{q+1,r}, \tag{24}$$

where $R_i^{q+1,r}$ is the residual, *i.e.* the numerical value of the left-hand side of Equation (22) calculated at the previous iteration. We use the value of h_M from the previous time step as the first approximation of the solution. The iterations are stopped when the maximum difference of the potential head values in the macroscopic equation are less than the required error tolerance.

3.5. Solving the micro-scale equations

At each macroscopic iteration, the micro-scale equation for flow in the aggregates has to be solved twice for each macroscopic grid cell. Equation (5) represents a general case of three-dimensional flow. However, since gravity is neglected and the potential at the outer surface of the aggregate is assumed to be uniform, the flow can be described with reasonable accuracy as a one-dimensional process. It is assumed that the potential and water content depend primarily on the distance from the outer surface of the aggregate. This approach has been introduced to simulate flow in fractured rocks and is known as Multiple Interacting Continua or MINC [8]. The aggregate is divided into a set of concentric shells (see Figure 1) and it is assumed that potential h_m is constant within each shell. A balance equation is formulated for each shell along the lines of the finite volume approach:

$$v_p \frac{\theta_{(m)p}^{q+1} - \theta_{(m)p}^q}{\Delta t} - s_{p+1/2} \frac{1}{2} \left(K_{(m)p+1}^{q+1} + K_{(m)p}^{q+1} \right) \frac{h_{(m)p+1}^{q+1} - h_{(m)p}^{q+1}}{\Delta x'} +$$
$$+ s_{p-1/2} \frac{1}{2} \left(K_{(m)p-1}^{q+1} + K_{(m)p}^{q+1} \right) \frac{h_{(m)p}^{q+1} - h_{(m)p-1}^{q+1}}{\Delta x'} = 0, \tag{25}$$

where p is the spatial index related to the microscopic spatial variable x', v_p is the volume of the corresponding grid block and $s_{p\pm1/2}$ are the block's external surfaces. The boundary condition applied at the external surface is $h_m(x,z,x',t) = h_M(x,z,t)$, while we have the $\partial h_m/\partial x' = 0$ symmetry condition at the aggregate's centre.

The resulting set of linear equations resembles that obtained by discretization of the one-dimensional flow equation in spherical coordinates. Numerical experiments presented in [14] demonstrate that the error introduced by the MINC approximation with respect to full 2D or 3D solutions is negligible. Equation (25)

is solved with an iterative procedure similar to that employed for the macroscopic equation.

4. Examples

4.1. Example 1

The purpose of the first example is to verify the numerical algorithm, especially the spatial discretization method, by comparison with an analytical solution. Since no analytical solutions exist for double-porosity media, we have to consider a simple case of homogeneous soil, *i.e.* we introduce $K^{\text{eff}} = K_M$, $f_M = 1.0$, $f_m = 0.0$ and $Q = 0$ in Equation (2). The chosen test case is widely used as a benchmark for verification of numerical codes [13]. It concerns one-dimensional vertical infiltration into a soil profile. The soil constitutive functions are given by the van Genuchten [15] formulae:

$$\theta(h) = \theta_R + (\theta_S - \theta_R) \left[1 + (\alpha_v|h|)^{n_v} \right]^{-m_v}, \qquad (26a)$$

$$K(h) = K_S \left[1 - (\alpha_v|h|)^{n_v-1} [1 + (\alpha_v|h|)^{n_v}]^{-m_v} \right]^2 [1 + (\alpha_v|h|)^{n_v}]^{-m_v/2}, \qquad (26b)$$

where θ_S is the water content at saturation, θ_R is the residual water content, K_S is the hydraulic conductivity at saturation, α_v and n_v are parameters related to the soil type and $m_v = 1 - 1/n_v$. The parameter values are shown in Table 1. The soil had an initial uniform potential of $h_{M,0} = -1000$ cm (Figure 5a). At the surface the value of $h_M = -75$ cm was imposed.

Table 1. Parameters of the constitutive relationships used in the examples

Parameter	θ_S	θ_R	α_v	n_v	K_S
Unit	$[-]$	$[-]$	$[\text{m}^{-1}]$	$[-]$	$[\text{m/h}]$
Example 1	0.368	0.102	3.35	2.00	0.33
Example 2 (macroporous region)	0.430	0.045	14.50	2.68	0.30
Example 2 (microporous region)	0.430	0.089	1.00	1.23	$7.00 \cdot 10^{-5}$

The numerical simulations were performed for a rectangular domain of 40×10 cm (Figure 5a). We used two numerical grids: a coarse one with 958 cells (average cell size of 1 cm) and a fine one with 3714 cells (average cell size of 0.5 cm). The time step varied in the range from 10^{-12} h to 0.02 h. Error tolerance for the iterative solver was specified using a mixed absolute/relative criterion: $\Delta h = 0.1$ cm $+ 0.005|h|$. The same tolerance was used for macro-scale and micro-scale equations.

The pressure profiles after 1 hour and 6 hours of infiltration are shown in Figure 5b; the reconstructed values at grid vertices along the $x = 0$ line are marked with points. The solid line represents Philip's analytical solution [16–18]. The numerical solution converges with the analytical one as the grid size is reduced.

4.2. Example 2

Our second example shows the numerical code's capability of simulating water flow in double-porosity soils in an irregular domain. We consider a vertical cross-section of a hill-slope with variable inclination (see Figure 6a). The soil has double-porosity structure with 10 cm cubic aggregates (see Figure 1). The aggregates' volumetric fraction is $f_m = 0.8$. The two materials' parameters, given in Table 1,
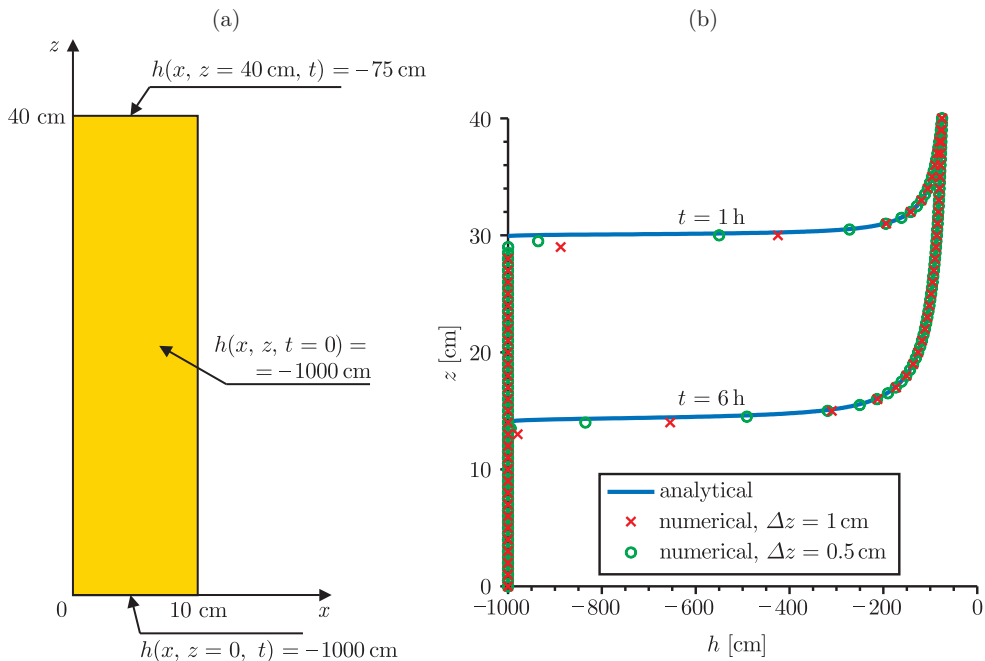
Figure 5. Example 1: (a) initial and boundary conditions;
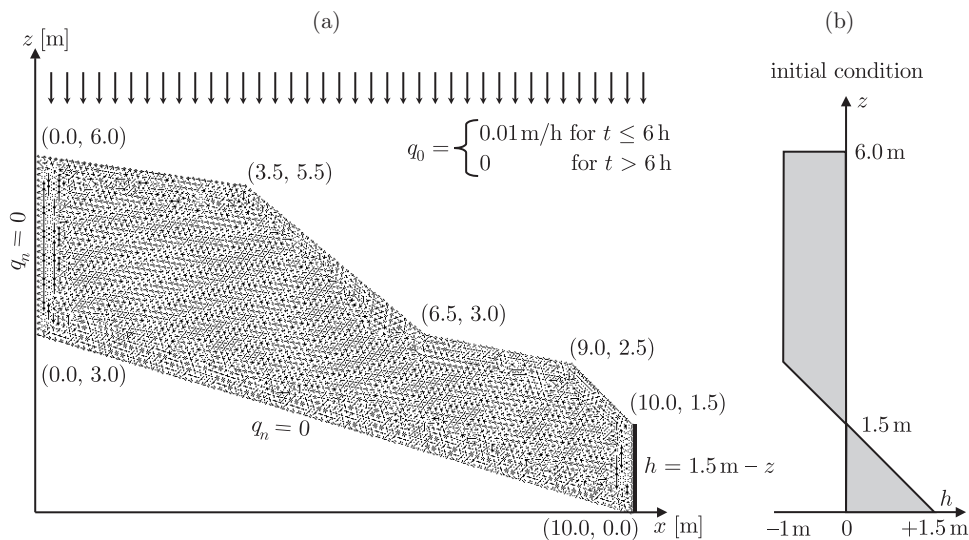(b) comparison of numerical results with Philip's analytical solution

Figure 6. Example 2: (a) numerical grid and boundary conditions;
(b) initial distribution of the water potential head

are respectively representative for coarse-textured and fine-textured soils. The slope
is drained by a stream located in the lower part of the right-hand boundary. The
water level in the stream is assumed to be constant and equal to 1.5 m above the
reference level. The initial distribution of the soil water potential is non-uniform and
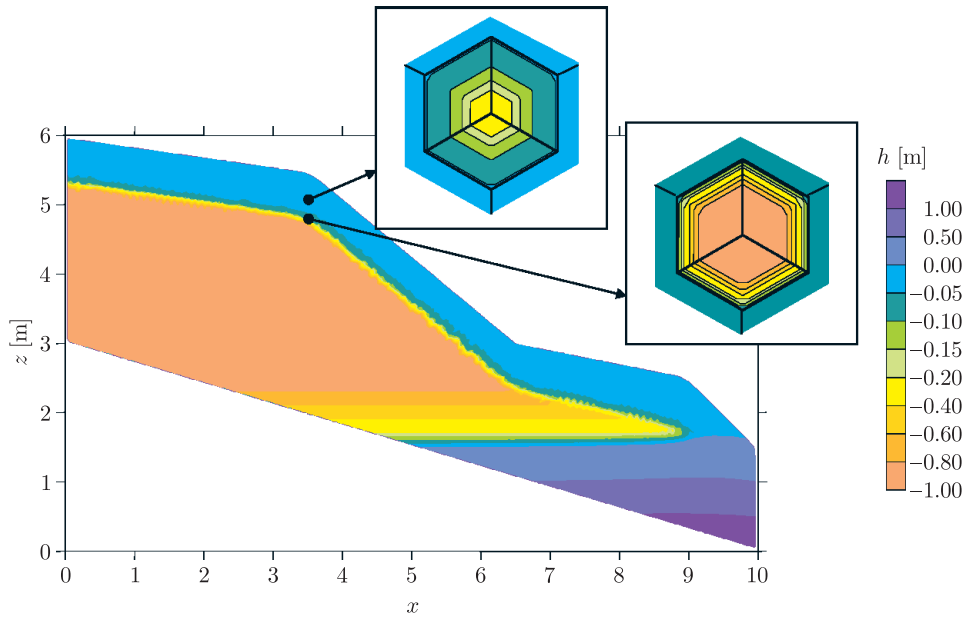
Figure 7. Example 2: distribution of the potential head in the macroporous system, $t = 6\,\mathrm{h}$; the insets show micro-scale variability of the potential head in the aggregates at two selected macroscopic points
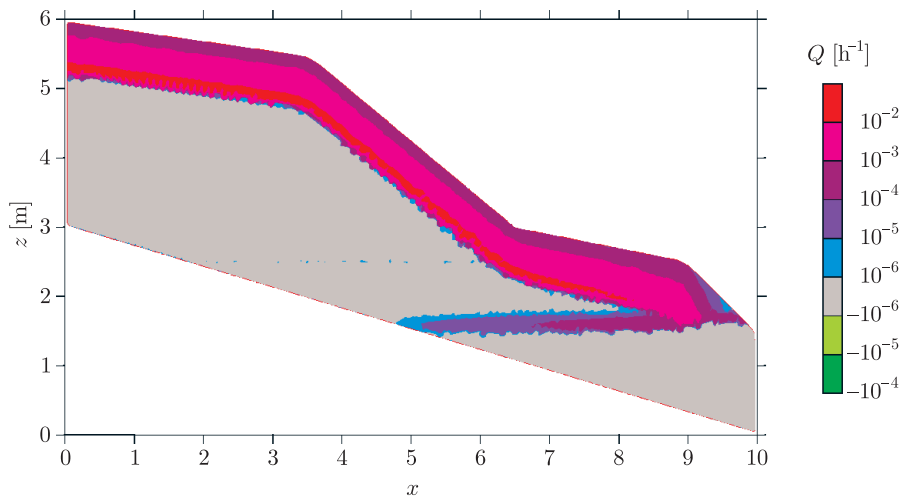

Figure 8. Example 2: spatial distribution of the values of source term Q, representing the intensity of water transfer between macroporous and microporous regions. Results for $t = 6\,\mathrm{h}$

depends on elevation (see Figure 6b). A linearly variable distribution is assumed in the lower part of the slope, corresponding to the hydrostatic conditions which occur near the stream. In the upper part of the slope ($z > 2.5\,\mathrm{m}$), a constant initial value is assumed, $h_0 = -1\,\mathrm{m}$, equal to the so-called water field capacity. The same value has been assumed for macroporous and microporous regions, but due to the differences in the $\theta(h)$ functions, the corresponding water contents in the two materials are different:
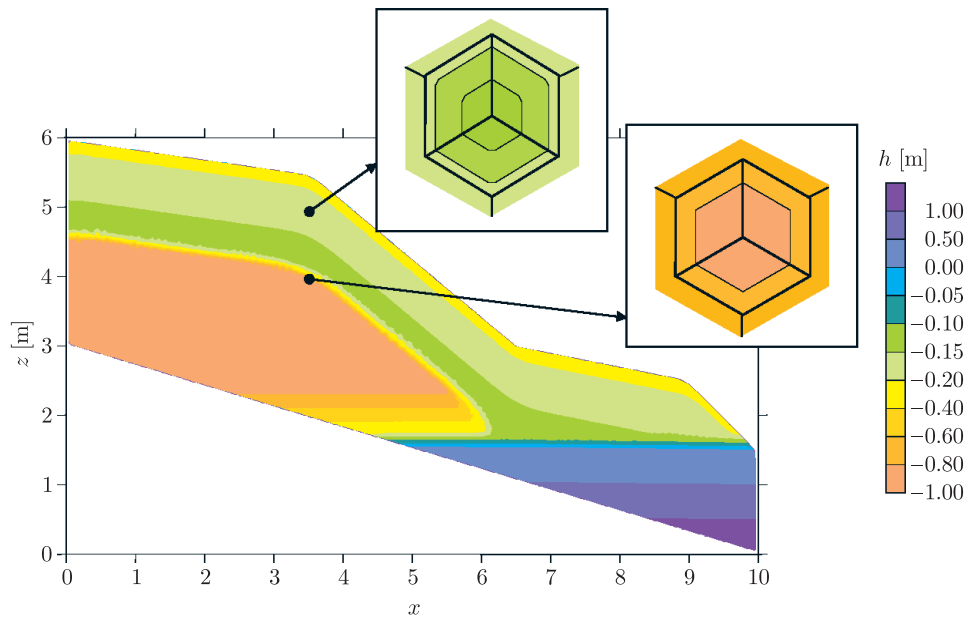
Figure 9. Example 2: distribution of the potential head in the macroporous system, $t = 72$h.
The insets show micro-scale variability of the potential head in the aggregates
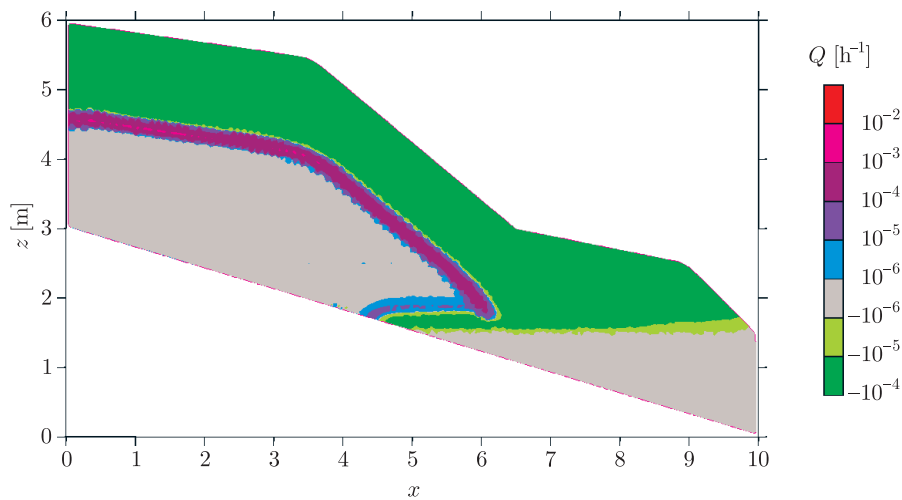at two selected macroscopic points

Figure 10. Example 2: spatial distribution of the values of source term Q, representing
the intensity of water transfer between macroporous and microporous regions.
Results for $t = 72$h

0.049 in the macroporous region, 0.388 in the aggregates. Such type of potential distribution is a reasonable approximation of natural conditions. We have assumed no-flow boundary conditions at the bottom (due to the presence of an impermeable layer) and at the left-hand side (due to symmetry). The upper surface of the slope is subject to infiltration by rainfall; the effective rainfall intensity has been assumed equal $q_0 = 0.01$m/h. The actual intensity of infiltration depends on slope inclination,

$q_n = q_0 \cos\phi$, where ϕ is the inclination angle. The rain duration is 6 hours, following which it is assumed that $q_0 = 0$, *i.e.* evaporation is neglected.

The simulation was performed using the grid shown in Figure 6a, consisting of 7104 cells of the average size of about 0.1m. At the microscopic level, the cubic aggregates were discretized with 11 grid blocks ("shells"). The limit values of time step and error tolerance were the same as in Example 1.

The results of the simulation are shown in Figures 7–10. The distribution of the soil water potential in the macroporous region at the end of the infiltration phase is presented in Figure 7 ($t = 6$h). In the upper part of the slope, just below the surface, the potential reaches values close to zero, *i.e.* the soil is nearly saturated. The wet and dry zones are separated by a sharp infiltration front. The insets show micro-scale distributions of the water potential inside the aggregates at two selected macroscopic cells. The potential is non-uniform and close to the initial value in the central part of the aggregate. The weakly conductive aggregates require relatively long time to reach a potential equilibrium with the surrounding highly conductive material. The intensity of water transfer from the macroporous region to the aggregates for the same time $t = 6$h is shown in Figure 8. The transfer rate is the highest at the wetting front and is gradually reduced behind it. Water transfer can also be observed in the vicinity of the groundwater table ($z = 1.5$m), because the water table elevation inside the slope has risen slightly due to infiltration.

After the rainfall, the water inside the hill-slope is subject to redistribution due to the force of gravity; the potential and transfer intensity for time $t = 72$h are shown in Figures 9 and 10. The water moves towards the groundwater table and the upper part becomes dry. Compared with the previous figures, the wet zone is wider, but the maximum value of the potential is lower. We can also observe negative values of transfer intensity, which means that now the aggregates release water to the macroporous regions. As can be seen in the insets, the micro-scale differences of potential inside the aggregates are now much smaller than during the infiltration phase. At the wetting front, the potential at the aggregates' surface is greater than in their centers, but the opposite situation is the case in the upper part of the slope. There, the potential at the aggregates' surface decreases relatively quickly due to drainage of the macroporous region, while it is greater on the inside. Thus, the direction of water transfer is from the aggregates to the macroporous regions. The above results demonstrate how aggregates act as a source or sink term for highly conductive macroporous systems.

5. Conclusions

A numerical approach to solving a two-scale model describing flow in structured soils has been presented. The macroscopic equation is two-dimensional and is solved on an unstructured grid with a cell-centered finite volume scheme. The microscopic flow in aggregates is modeled using a one-dimensional approximation (MINC). The solutions at the two scales are coupled using an iterative procedure. The examples show that the proposed algorithm is suitable for modeling flow in structured porous media. The approach can be extended to account for macroscopic-scale heterogeneity and anisotropy of soils.

Acknowledgements

References

[1] Douglas J J and Arbogast T 1990 *Dual Porosity Models for Flow in Naturally Fractured Reservoirs* (Cushman J H *et al.*, Eds) Dynamics of Fluids in Hierarchical Porous Media, Academic Press, London

[2] Lewandowska J, Szymkiewicz A, Burzyński K and Vauclin M 2004 *Advances in Water Resources* **27** 283

[3] Szymkiewicz A and Lewandowska J 2006 *Hydrological Sciences Journal* **51** 1106

[4] Arbogast T 1997 *Computational Aspects of Dual-porosity Models* (Hornung U, Ed.), Homogenization and porous media, Springer, New York 203

[5] Szymkiewicz A, Lewandowska J, Angulo-Jaramillo R and Butlańska J *Two-scale Modeling of Unsaturated Water Flow in the Double-porosity Medium under Axi-symmetrical Conditions* (submitted)

[6] Manzini G and Ferraris S 2004 *Advances in Water Resources* **27** 1199

[7] Lewandowska J and Laurent J-P 2001 *Transport in Porous Media* **45** 321

[8] Lewandowska J, Szymkiewicz A and Boutin C 2005 *Modeling of Unsaturated Hydraulic Conductivity of Double Porosity Soils* Actes de 17ème Congrès Français de Mécanique, Troyes

[9] Pruess K and Narasimhan T 1985 *Society of Petroleum Engineers Journal* **25** 14

[10] Bertolazzi E and Manzini G 2005 *Computers and Mathematics with Applications* **49** 1755

[11] Pasdunkorale J A and Turner I W 2005 *Journal of Computational Mathematics* **23** 1

[12] Belfort B and Lehmann F 2005 *Vadose Zone Journal* **4** 1191

[13] Celia M A, Bouloutas E T and Zarba R L 1990 *Water Resources Research* **26** 1483

[14] Lai C-H and Liu C-W 2001 *Proc. National Science Council Republic of China (A)* **25** 35

[15] van Genuchten M Th 1980 *Soil Science Society of America Journal* **44** 892

[16] Philip J R 1957 *Soil Science* **83** 345

[17] Philip J R 1957 *Soil Science* **83** 435

[18] Philip J R 1957 *Soil Science* **84** 163